Molecular Cell
Article

Structure and Biological Importance of the Spn1-Spt6 Interaction, and Its Regulatory Role in Nucleosome Binding

Seth M. McDonald,[1,2] Devin Close,[1,2,3] Hua Xin,[1] Tim Formosa,[1,*] and Christopher P. Hill[1,*]
[1]Department of Biochemistry, University of Utah School of Medicine, Salt Lake City, UT 84112-5650, USA
[2]These authors contributed equally to this work
[3]Present address: Bioscience Division, Los Alamos National Laboratory, Los Alamos, NM 87545, USA
*Correspondence: tim@biochem.utah.edu (T.F.), chris@biochem.utah.edu (C.P.H.)
DOI 10.1016/j.molcel.2010.11.014

SUMMARY

Eukaryotic transcription and mRNA processing depend upon the coordinated interactions of many proteins, including Spn1 and Spt6, which are conserved across eukaryotes, are essential for viability, and associate with each other in some of their biologically important contexts. Here we report crystal structures of the Spn1 core alone and in complex with the binding determinant of Spt6. Mutating interface residues greatly diminishes binding in vitro and causes strong phenotypes in vivo, including a defect in maintaining repressive chromatin. Overexpression of Spn1 partially suppresses the defects caused by an *spt6* mutation affecting the Spn1 interface, indicating that the Spn1-Spt6 interaction is important for managing chromatin. Spt6 binds nucleosomes directly in vitro, and this interaction is blocked by Spn1, providing further mechanistic insight into the function of the interaction. These data thereby reveal the structural and biochemical bases of molecular interactions that function in the maintenance of chromatin structure.

INTRODUCTION

Spn1 and Spt6 are transcription factors that interact with one another and are each essential for viability in yeast (Clark-Adams and Winston, 1987; Fischbeck et al., 2002). *S. cerevisiae* Spn1 is a 410 residue, 46 kDa protein with a central core domain (residues 140–300) that is flanked on both sides by regions that are predicted to be disordered (Ward et al., 2004). Spt6 is a 1451 residue, 168 kDa protein whose core (residues 300–1250) likely resembles the structure of the bacterial Tex protein (Johnson et al., 2008) with an acidic N-terminal extension that is expected to be unstructured (Ward et al., 2004) and a C-terminal domain (CTD) that adopts an SH2 fold (Dengl et al., 2009; Maclennan and Shaw, 1993). Spn1 and Spt6 interact stably with one another, and they and their interaction have been implicated in several aspects of gene expression (Krogan et al., 2002; Lindstrom et al., 2003; Yoh et al., 2007; Yoh et al., 2008).

Spt6 was originally identified in a screen for factors that alter normal initiation of transcription (Clark-Adams and Winston, 1987; Denis, 1984; Neigeborn et al., 1987; Simchen et al., 1984). Subsequently, Spt6 was implicated in a variety of biological processes in organisms ranging from yeasts to humans, including embryogenesis in Zebrafish (Keegan et al., 2002; Kok et al., 2007), multiple stages of development in *Drosophila* (Ardehali et al., 2009), gut morphogenesis in *C. elegans* (Nishiwaki et al., 1993), signal transduction in mammals (Baniahmad et al., 1995; Shen et al., 2009), and HIV transcription regulation and mRNA processing in human cells (Vanti et al., 2009; Yoh et al., 2007). The role in transcription initiation has been ascribed to the ability of Spt6 to chaperone histones to promote reassembly of nucleosomes in the wake of RNA polymerase II (RNAPII), thereby reestablishing the default repressive chromatin state that prevents inappropriate initiation of transcription (Adkins and Tyler, 2006; Bortvin and Winston, 1996; Cheung et al., 2008; Kaplan et al., 2003). While of profound importance, maintaining repressive chromatin appears to be just one of Spt6's roles. For example, Spt6 also promotes elongation by RNAPII (Hartzog et al., 1998; Kaplan et al., 2005; Kaplan et al., 2000; Lindstrom et al., 2003) on nucleosome-free DNA templates in vitro (Endoh et al., 2004; Hartzog et al., 1998; Keegan et al., 2002; Yoh et al., 2007), as well as on chromatin templates in vivo (Ardehali et al., 2009). Together, these data indicate that Spt6 plays a number of mechanistically distinct roles during transcription.

The *SPN1* gene was originally identified as a key regulator of transcription from genes that are regulated postrecruitment of RNAPII (Fischbeck et al., 2002). Spn1 was also identified as a protein that interacts with Spt6 and has been reported to bind with Spt6 in some but not all of Spt6's functional states (Lindstrom et al., 2003; Yoh et al., 2007; Zhang et al., 2008). For example, Spt6 can be coimmunopurified with three distinct Spt4/5-RNAPII complexes, whereas Spn1 is found in only two of these complexes (Lindstrom et al., 2003). The *CYC1* gene of *S. cerevisiae* provides an example of how the Spn1-Spt6 interaction contributes to postrecruitment regulation (Zhang et al., 2008). RNAPII is constitutively bound to the *CYC1* promoter, but is kept from elongating because it interacts with Spn1, which in turn inhibits the Swi/Snf nucleosome remodeling

complex from promoting transcription. During activation, Spt6 binds to Spn1, and repression of Swi/Snf recruitment is relieved.

Spn1 is also needed to achieve normal recruitment of the histone methyltransferase HYPB/Setd2 (Yoh et al., 2008) and the elongation factor TFIIS (Ling et al., 2006; Zhang et al., 2008) to RNAPII complexes traversing active genes. HYPB/Setd2 methylates histone H3K36, which in turn recruits Rpd3-type histone deacetylases to restore chromatin to the repressive hypoacetylated state and block inappropriate transcription (Yoh et al., 2008). In contrast to their antagonistic relationship in activating postrecruitment initiation, Spn1 and Spt6 each contribute toward restoration of repressive chromatin. Human Spn1/IWS1 also binds the protein arginine methyltransferase PRMT5, which methylates the elongation factor Spt5 and thereby regulates its interaction with RNAPII (Liu et al., 2007). Spn1 can additionally function through interactions with pathway-specific regulatory factors, such as the *Arabidopsis* steroid hormone responsive transcription factor BES1, which recruits Spn1 to the promoter and transcribed regions of activated genes (Li et al., 2010). Spn1 therefore contributes in several ways to the appropriate functioning of RNAPII.

In addition to their roles in regulating transcription, Spt6 and Spn1 also collaborate to promote mRNA processing and export. Spt6 is required for proper 3′ end formation by preventing premature 3′ processing at upstream polyadenylation signals (Bucheli and Buratowski, 2005; Kaplan et al., 2005). Further, mammalian Spt6 can bind the Ser2-phosphorylated RNAPII CTD, enhancing recruitment of RNA processing/export factors (Yoh et al., 2007, 2008), and *Drosophila* Spt6 copurifies with the RNA processing exosome complex (Andrulis et al., 2002). Both *SPN1* and *SPT6* have also been implicated in mRNA splicing in *S. cerevisiae* (Burckin et al., 2005), and binding of human Spn1/IWS1 to the RNA export factor REF1/Aly is important for recruitment of REF1/Aly to the body of the *c-Myc* gene during transcription (Yoh et al., 2007).

Spt6 and Spn1 and their interaction with one another therefore play pivotal roles in defining the composition of RNAPII elongation complexes, maintaining the structure of chromatin, and modulating the production of mature mRNA transcripts. To advance mechanistic understanding of their functions, we have determined the structural basis of the Spn1-Spt6 interaction. We also demonstrate the importance of this interface in vitro and in vivo, and show that Spn1 negatively regulates binding of Spt6 to nucleosomes.

RESULTS

Mapping of the Spn1-Spt6 Interface

Full-length *S. cerevisiae* Spt6 and Spn1 proteins were poorly behaved, but deletion of much of their presumably unstructured N-terminal regions (Ward et al., 2004) allowed us to observe coelution of a complex of recombinant Spn1(120–410) and Spt6(206–1451) by size-exclusion chromatography in sodium chloride concentrations up to 300 mM (data not shown). Spt6 (239–1451) also bound Spn1, whereas Spt6(315–1451) did not. Further truncations revealed that Spt6(239–268) is sufficient for Spn1 binding (Figures 1A and 1B). This 30 residue segment of Spt6 is predicted to be unstructured, and comes from a region that is N-terminal to the region expected to resemble the structure of the bacterial protein Tex (Johnson et al., 2008). Spn1 (148–293) includes most of the Spn1 residues that are predicted to be structured and retained the ability to bind Spt6. The slightly larger Spn1(141–305) fragment was previously shown to complement a deletion of *SPN1* (Fischbeck et al., 2002), indicating that this core domain provides the major function(s) of Spn1 in vivo. Isothermal titration calorimetry (ITC) was used to measure binding affinities of Spn1(148–293) for two different Spt6 constructs: Spt6(239–1117), the largest Spt6 construct that remained soluble at sufficient concentrations for these experiments, and Spt6(239–268), the smallest construct tried that retained full binding affinity. In both cases the binding displayed 1:1 stoichiometry and the mean binding constant (K_D) was 170 nM (Figures 1C and 1D and see Table S1 available online). This indicates that the 30 residue segment of Spt6, Spt6 (239–268), is sufficient to recapitulate the binding energy observed for larger Spt6 constructs.

Crystal Structures of the Spn1 Core

The crystal structure of Spn1(148–307) was determined by the single-wavelength anomalous diffraction method using data collected to 3.0 Å resolution from a selenomethionine-substituted crystal (Figure 2A, Table 1). This unrefined model was used in molecular replacement calculations with 2.15 Å data from a native crystal that belonged to a different space group, and the native structure was refined to R_{work}/R_{free} values of 18.5%/22.4%. Residues 148–295 were clearly observed in the electron density, as were four nonnative N-terminal residues that remained after TEV digestion. The 12 C-terminal residues were disordered and are not included in the final model.

Spn1(148–307) forms a right-handed superhelical bundle of eight helices (named H1–8, Figure 2A). Surprisingly, this structure resembles the domains of the RNA processing factors Pcf11 (*S. cerevisiae*) (Meinhart and Cramer, 2004) and SCAF8 (human) (Becker et al., 2008) that bind the RNAPII CTD (Figure S1A). Spn1 is reported to associate with RNAPII (Zhang et al., 2008), and the structural similarity suggested that Spn1 might bind the RNAPII CTD. We have not, however, observed binding in a fluorescence polarization assay between the Spn1 core and synthetic peptides, either phosphorylated or unphosphoryalated, that span more than two heptad repeats of the RNAPII CTD (data not shown).

Crystal Structure of an Spn1-Spt6 Complex

The structure of an Spn1(148–293):Spt6(239–268) complex was determined by molecular replacement and refined to R_{work}/R_{free} values of 18.6%/24.4% against 2.15 Å resolution data (Figure 2B, Figure S2, Table 1). There are two complexes in the asymmetric unit that superimpose closely with an rmsd of ~0.5 Å over all 170 native ordered Cα atoms. Residues 148–292 of Spn1 are clearly visible in the electron density, as are six nonnative N-terminal residues that remain after TEV digestion. Residues 239–263 of Spt6 are also clearly defined in the electron density as well as four nonnative N-terminal residues. There is no clear electron density for the five C-terminal residues of Spt6 and the one C-terminal residue of Spn1, and these are

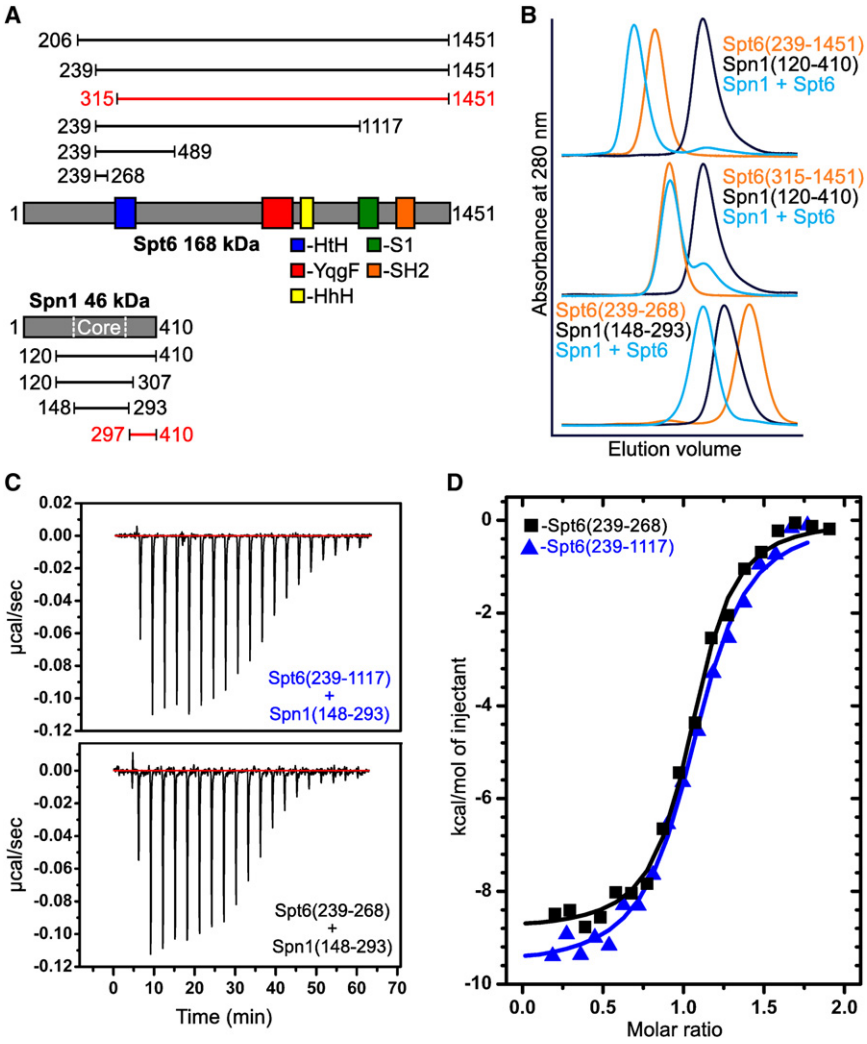

Figure 1. The Spn1 Core Binds 30 Residues in the Spt6 N-Terminal Region

(A) Spt6 and Spn1 domain organization and their interacting regions. Constructs assayed for binding are indicated above (Spt6) or below (Spn1) with their N- and C-terminal residues given. Constructs that showed binding are colored black, while those that did not show binding are colored red.

(B) Overlays of size-exclusion chromatograms with Spn1 in black, Spt6 in orange, and binding experiments in blue. Chromatograms are scaled on the y axis to allow comparison of the elution volume profiles of each protein or binding experiment. Spn1 has a 6-fold lower molar extinction coefficient, and so at equimolar concentrations, the Spn1 peak appears approximately six times smaller than the Spt6 peak (blue, middle panel). The x axis shows the 50–100 ml elution volume.

(C) Raw ITC data of the titration of Spn1(148–293) into Spt6(239–1117) (top) and the titration of Spt6 (239–268) into Spn1(148–293) (bottom).

(D) Representative binding isotherms of the titration experiments from (C). See text and Table S1 for thermodynamic parameters.

not included in the final model. Spn1 retains the same globular eight helix-bundle fold in the complex, showing no notable conformational changes upon binding Spt6 (rmsd ~0.5 Å on 135/145 pairs of Cα atoms). Binding of Spt6 to Spn1 does not mimic the binding of RNAPII CTD peptides to Pcf11/SCAF8, as it involves a face of Spn1 that is structurally distinct from the binding surface of Pcf11/SCAF8 (Figure S1B).

The structure of the Spn1(148–293):Spt6(239–268) complex reveals an extensive interface in which the Spt6 residues drape across the structured Spn1 core domain as two helices, H1 (residues 239–249) and H2 (256–265), that are connected by a short extended segment. There are multiple contacts along the length of the Spt6 segment that bury a total of 1790 Å^2 of accessible surface area upon complex formation. Spt6 H1 and the connecting segment, in particular, include a high fraction of conserved residues and contact a conserved patch on the Spn1 surface, thereby indicating that this interface is likely to be preserved across eukaryotes (Figures 2C–2E, Figures S1C and S1D).

Distinctive hydrophobic and polar interactions are made throughout the length of the Spt6 peptide (Figure 3). Starting at the Spt6 peptide N terminus, the H1 residues M245, I248, and F249 contact a hydrophobic pocket formed by Spn1 residues L256, G262, I266, I286, and W289. The C-terminal carbonyl groups of Spt6 H1 form water-mediated hydrogen bonds with Spn1 R263 guanidinium, whose extensive network of contacts also includes direct hydrogen bonds with the carboxylate of D254 in the extended region of Spt6. The aromatic side chain of Spt6 Y255, from the extended central region, makes van der Waals contacts with Spn1 P227, V264, and F267, while its hydroxyl group forms a hydrogen bond with the carboxylate of Spn1 E226. The Spt6 H2 residues W257, A258, L259, and I261 contact two hydrophobic patches formed by Spn1 P227, G231, V264, and F267. Finally, the Spt6 E262 carboxylate hydrogen bonds with Spn1 S271 and R273, and K272 forms polar contacts with the amide of Spt6 N263. These extensive interactions are consistent with the strong specific binding observed between Spn1 and Spt6.

Mutations that Disrupt Spn1-Spt6 Complex Formation In Vitro

To validate the relevance of the interface seen in the crystal structure, Spn1(148–293) and Spt6(239–268) variants were expressed and purified, and binding affinities were measured by ITC (Figure 4, Figure S3, Table S1). The Spt6-F249K protein bound Spn1 with a mean K_D of 11 μM, a reduction in affinity compared to the WT interaction of about 60-fold. The affinity of the Spn1-R263D protein for Spt6 (mean K_D of 30 μM) was reduced about 170-fold compared to WT. No binding was

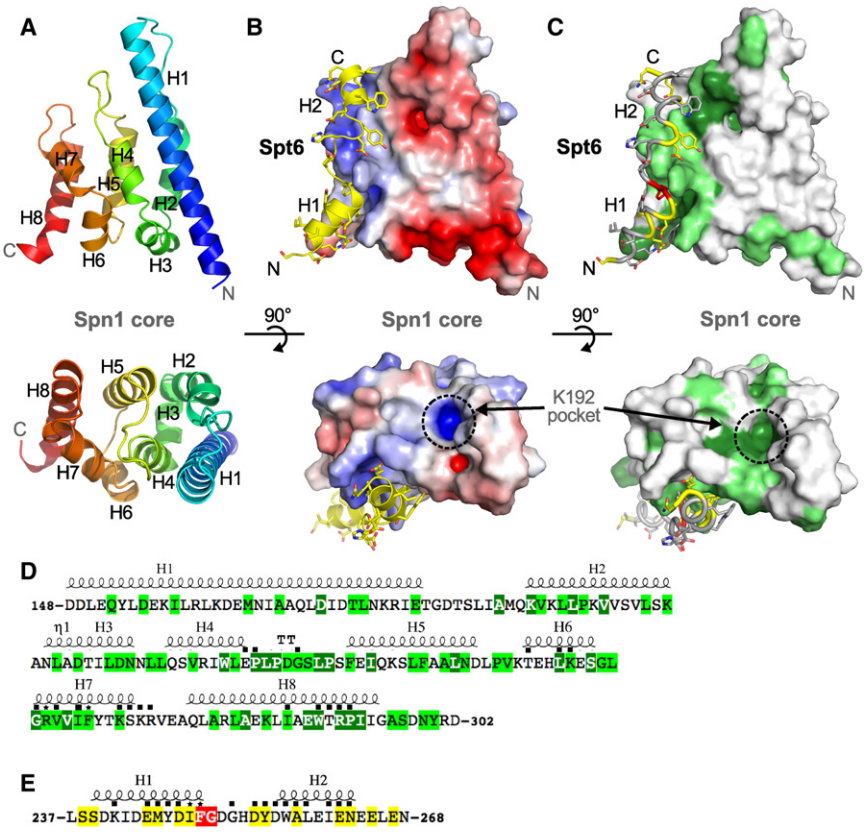

Figure 2. Structures of the Spn1 Core and Its Complex with Spt6

(A) The structure of the Spn1 core shown as a cartoon representation in two orthogonal views. The polypeptide chain is colored as a blue to red rainbow from N to C terminus. Secondary structures and the N and C termini are labeled.

(B) Structure of the Spn1-Spt6 complex. The Spn1 core is shown as a surface electrostatic (±5 kT/e) representation in the same views as (A). Spt6 is colored yellow and the N and C termini and the helices are labeled. Spn1 K192 has been implicated in interactions with RNAPII (Zhang et al., 2008) and lies in the basic conserved pocket indicated. Remnants of the affinity tags that remain in the crystallized Spn1 and Spt6 proteins are not shown in any of the figures and do not contribute to the Spn1 interface.

(C) Same as (B), except that the Spn1 surface and Spt6 peptide are colored according to conservation.

(D) Spn1 core amino acid sequence. Secondary structural elements are indicated above, and were defined with ESPript (Gouet et al., 2003). Residues that make direct contact across the interface are indicated with a black square or with an asterisk if they were mutated in this study. Numbering and residue identities shown here refer to the *S. cerevisiae* protein. Coloring represents degrees of conservation, dark green (high), light green (medium), in an alignment of proteins from *Saccharomyces cerevisiae*, *Schizosaccharomyces pombe*, *Caenorhabditis elegans*, *Drosophila melanogaster*, *Danio rerio*, and *Homo sapiens*. Amino acid sequences were aligned using the T-coffee multiple sequence alignment method (Notredame et al., 2000) and slightly adjusted manually in light of the structure (Figure S2).

(E) Same as (D) but for Spt6. High conservation (red), medium conservation (yellow).

detected for the Spn1-F267E protein at concentrations expected to give a reliable estimate of affinity around 40 μM. These observations validate the crystallographic interface and demonstrate that single point mutations are sufficient to significantly reduce binding affinity in vitro.

Mutating the Spn1-Spt6 Interface Causes Profound Effects In Vivo

To determine the physiological importance of the Spn1-Spt6 interaction, we introduced *spt6-F249K*, *spn1-R263D*, and *spn1-F267E* mutations into the genomes of yeast cells such that each mutant protein was expressed from its native promoter as the sole source of the affected protein. *spt6-F249K* caused a moderate growth defect at low temperatures, and this was strongly enhanced at elevated temperatures (Figure 5A). Strains with the *spn1-R263D* mutation grew normally at all temperatures, while those with the *spn1-F267E* mutation were normal at low temperatures but failed to grow at high temperatures. Each of the three mutations caused a defect in transcription initiation site selection due to defective chromatin repression, as indicated by the Spt$^-$ phenotype (growth of a strain with the *lys2-128∂* allele on medium lacking lysine (Simchen et al., 1984; Figures 5A–5C). The strength of the defect was different for each mutation, being weakest for *spt6-F249K*, stronger for *spn1-R263D*, and strongest for *spn1-F267E*. This order correlates precisely with the level of perturbation of binding observed with these mutant proteins in vitro (Figure 4, Table S1), strongly supporting the importance of the Spn1-Spt6 binding interface detected in our crystal structure in maintaining a repressive chromatin state in vivo.

Each mutation in the Spn1-Spt6 binding interface disturbed the interaction to a different extent in vitro (Figure 4, Table S1), but each individual mutation was tolerated in vivo (Figure 5). If the phenotypes caused by individual mutations result from partial disruption of binding, then combining the mutations should lead to enhanced defects. Consistent with this prediction, cells with both *spt6-F249K* and *spn1-R263D* mutations were viable but severely impaired for growth (Figure 5A), and cells with both *spt6-F249K* and *spn1-F267E* were inviable (Figure S4D). The severity of the defect caused by combining mutations therefore correlates with the level of disruption of binding by the individual mutations, suggesting that the Spn1-Spt6 interaction is essential for viability. We were unable to detect an interaction between Spt6 and Spn1-F267E in vitro (Figure 4), but the viability of the *spn1-F267E* strain suggests that this mutant retains some binding. Combining *spt6-F249K* with *spn1-K192N* was also lethal (Figure S4D); this mutation does not directly affect the Spn1-Spt6 interface (Figures 2B and 2C) but has been shown to decrease the

Table 1. Data Collection and Refinement Statistics

	Spn1 Core SeMet	Spn1 Core Native	Spn1-Spt6 Complex
Data Collection			
Beamline	SSRL 9-2	Home source	Home source
Space group	$P3_112$	$P3_212$	$P2_12_12$
Unit cell dimensions			
a, *b*, *c* (Å)	61.9, 61.9, 240.4	61.3, 61.3, 116.05	105.9, 68.7, 73.9
α, β, γ (°)	90, 90, 120	90, 90, 120	90, 90, 90
Resolution (Å)	35–3.0	30–2.15	30–2.15
Wavelength (Å)	0.97923 (Peak)	1.54178	1.54178
I/σ_I	23.2 (2.8)	22 (4.1)	19.7 (3.1)
Completeness (%)	90.8 (92.3)	99.8 (98.4)	100.0 (100.0)
R_{sym} (%)	5.2 (47.6)	6.1 (31.9)	6.4 (54.4)
Redundancy	4.2 (4.1)	5.8 (3.8)	5.3 (5.0)
Refinement			
Resolution (Å)		29.6–2.15	27.7–2.15
Number of reflections		13,847	30,096
R_{work}/R_{free} (%)		18.5/22.4	18.6/24.4
Number of protein atoms		1,216	2,903
Number of solvent atoms		144	268
Rmsd bond lengths (Å)/angles (°)		0.007/1.001	0.012/1.279
φ/ψ most favored/allowed (%)		99.3/100.0	99.2/100.0

Values in parentheses are for the highest-resolution shell.

interaction between Spn1 and RNAPII (Zhang et al., 2008), and our results with the recombinantly expressed protein suggest that Spn1-K192N protein is unstable (data not shown). Synthetic growth defects therefore support the importance of the Spn1-Spt6 interaction, but defects outside this interface can also cause additive growth defects.

Another strategy for determining the importance of the Spn1-Spt6 interface is to test the effect of overexpressing one partner. If decreased affinity of Spt6-F249K protein for Spn1 is responsible for growth defects in vivo, these defects might be suppressed by increasing the level of Spn1 protein. We tested this by transforming an *spt6-F249K* strain with high-copy plasmids containing variants of *SPN1*. As shown in Figure 5C, increasing the level of normal *SPN1* suppressed the temperature sensitivity and partially corrected the Spt$^-$ phenotype caused by *spt6-F249K*. Consistent with retention of partial binding, overexpression of *spn1-R263D* also had an effect but suppressed less efficiently, rescuing growth at 36° but not at 38° and having no effect on the Spt$^-$ phenotype. Spn1-K192N is not active at elevated temperatures (Zhang et al., 2008; and Figure 5A), and overexpression of this allele also did not rescue the phenotypes caused by *spt6-F249K*. Elevated *SPN1* copy number did not suppress the temperature sensitivity or Spt$^-$ phenotypes caused by the *spt6-1004* allele (data not shown), which is a deletion of the helix-hairpin-helix domain within the Tex-like core of Spt6 (Kaplan et al., 2005). The suppression of *spt6* defects by increased Spn1 is therefore at least partly specific for a mutation that alters the Spn1-Spt6 interface, and supports the importance of this interaction in an essential function in vivo.

Spt6 Binds Nucleosomes Directly and Is Inhibited by Spn1

Spt6 has been shown to bind both $(H3\text{-}H4)_2$ tetramers and H2A-H2B dimers (Bortvin and Winston, 1996), leading to models in which Spt6 acts as a histone chaperone during nucleosome eviction and redeposition. Following our earlier prediction (Johnson et al., 2008) that the N-terminal region of Spt6 binds nucleosomes, we examined purified Spt6 constructs for nucleosome-binding activity in an electrophoretic mobility shift assay (EMSA). Interestingly, we found that intact Spt6 does bind nucleosomes in this assay (Figure 6), but does so only in the presence of the small HMGB family member Nhp6 (Stillman, 2010). This is similar to the requirement for addition of Nhp6 to observe complexes between nucleosomes and a different histone chaperone, FACT (Formosa et al., 2001). As with FACT, this suggests that Spt6 may form stable complexes with nucleosomes only after the nucleosome has been partially destabilized by Nhp6. This requirement appears to be physiologically relevant, because loss of Nhp6 in vivo exacerbated the growth defects caused by any of several mutations in Spt6 (Figure 5C, Figure S4A). Histone chaperones do not necessarily bind intact nucleosomes; in fact, the Asf1-(H3-H4) interaction is incompatible with histone contacts within the nucleosome (Antczak et al., 2006; English et al., 2006; Natsume et al., 2007). Binding to both free histones and to nucleosomes therefore might indicate that Spt6 makes multiple distinct contacts with nucleosomes and their components during different steps in chromatin maintenance. Spt6(239–1451) bound nucleosomes while Spt6 (315–1451) did not (Figure 6, compare lanes 2 and 3). Thus, the

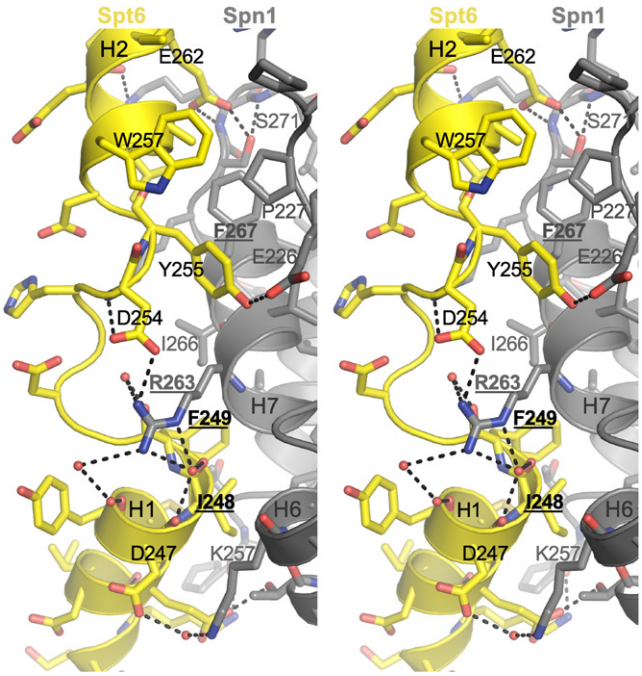

Figure 3. Details of the Spn1-Spt6 Interface

Stereoview of the Spn1-Spt6 interface. Residues mutated in this study are indicated in bold font and underlined. Water molecules are shown as red spheres, and polar interactions are indicated by black dashes.

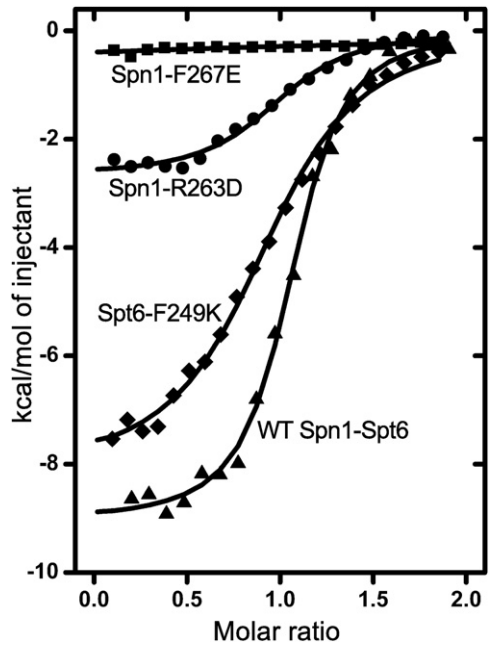

Figure 4. Mutations at the Spn1-Spt6 Interface Disrupt Binding In Vitro

Representative ITC binding isotherms for the indicated mutant Spt6(239–268) and Spn1(148–293) proteins, Spt6-F249K (diamonds), Spn1-R263D (circles), and Spn1-F267E (squares). A WT isotherm is shown for reference (triangles). See text and Table S1 for thermodynamic parameters.

region of Spt6 required for nucleosome binding (residues 239–314) contains the region required for Spn1 binding (239–268), suggesting that these two interactions may be mutually exclusive.

Consistent with this possibility, adding Spn1(120–410) to the nucleosome-binding assay inhibited the formation of Spt6-nucleosome complexes (Figure 6, compare lanes 2 and 5). Spn1 did not form stable complexes with nucleosomes itself, so the inhibition is unlikely to be caused by competition between Spn1 and Spt6 for a common binding site on nucleosomes. Spn1 did not interact with Nhp6 genetically (Figures S4B and S4C), and inhibition of Spt6-nucleosome complex formation by Spn1 could not be overcome by increasing the concentration of Nhp6 (data not shown), making it unlikely that the inhibition is caused by sequestering of Nhp6 by Spn1. Instead, Spn1 appears to prevent Spt6 from binding to nucleosomes directly by blocking the Spt6 binding domain. Supporting this interpretation, the Spn1-R263D variant with reduced affinity for Spt6 did not block formation of Spt6-nucleosome complexes efficiently (Figure 6, lane 7). Further, the Spt6-F249K mutation affects a region important for both nucleosome binding and Spn1 interaction (Figures 4 and 6, compare lanes 2 and 8). Spt6-F249K protein was impaired for nucleosome binding, but the residual binding was partially resistant to the addition of Spn1 (Figure 6, lanes 8 and 9). These results show that Spt6 residue F249 contributes to both nucleosome binding and to Spn1 binding, and that Spn1 binding can block an interaction between Spt6 and nucleosomes. The Spn1-Spt6 interaction can therefore provide a switch that controls the interaction of Spt6 with nucleosomes, and the proper functioning of this switch is important for maintaining normal chromatin structure.

DISCUSSION

We have determined a crystal structure of the ordered central domain of Spn1 and shown that it binds a 30 residue segment of Spt6. We have also determined a crystal structure of an Spn1-Spt6 complex that reveals that Spt6 binds in an extended/helical conformation that drapes the Spt6 residues along one face of Spn1. We further used site-directed mutations to disrupt this interaction and demonstrated that the interaction observed in solution depends on residues located at the interface seen in the crystal structure. Binding is not accompanied by conformational changes in Spn1. In contrast, Spt6(239–268) is almost certainly unstructured in isolation and becomes ordered upon binding Spn1. Indeed, the first 300 residues of Spt6 are likely to be unstructured in isolation (Ward et al., 2004), whereas much of the remainder of the protein appears to comprise multiple recognizable structural domains that likely fold against each other to form an elongated structure (Johnson et al., 2008). The extended and inherently flexible nature of the Spn1 binding sequence of Spt6 presumably explains why dramatic mutations in the interface substantially weaken but do not completely eliminate this interaction, as localized perturbations can be accommodated by conformational changes that do not propagate across the entire interface. Moreover, the ~35 residues separating the Spn1-binding residues from the ordered

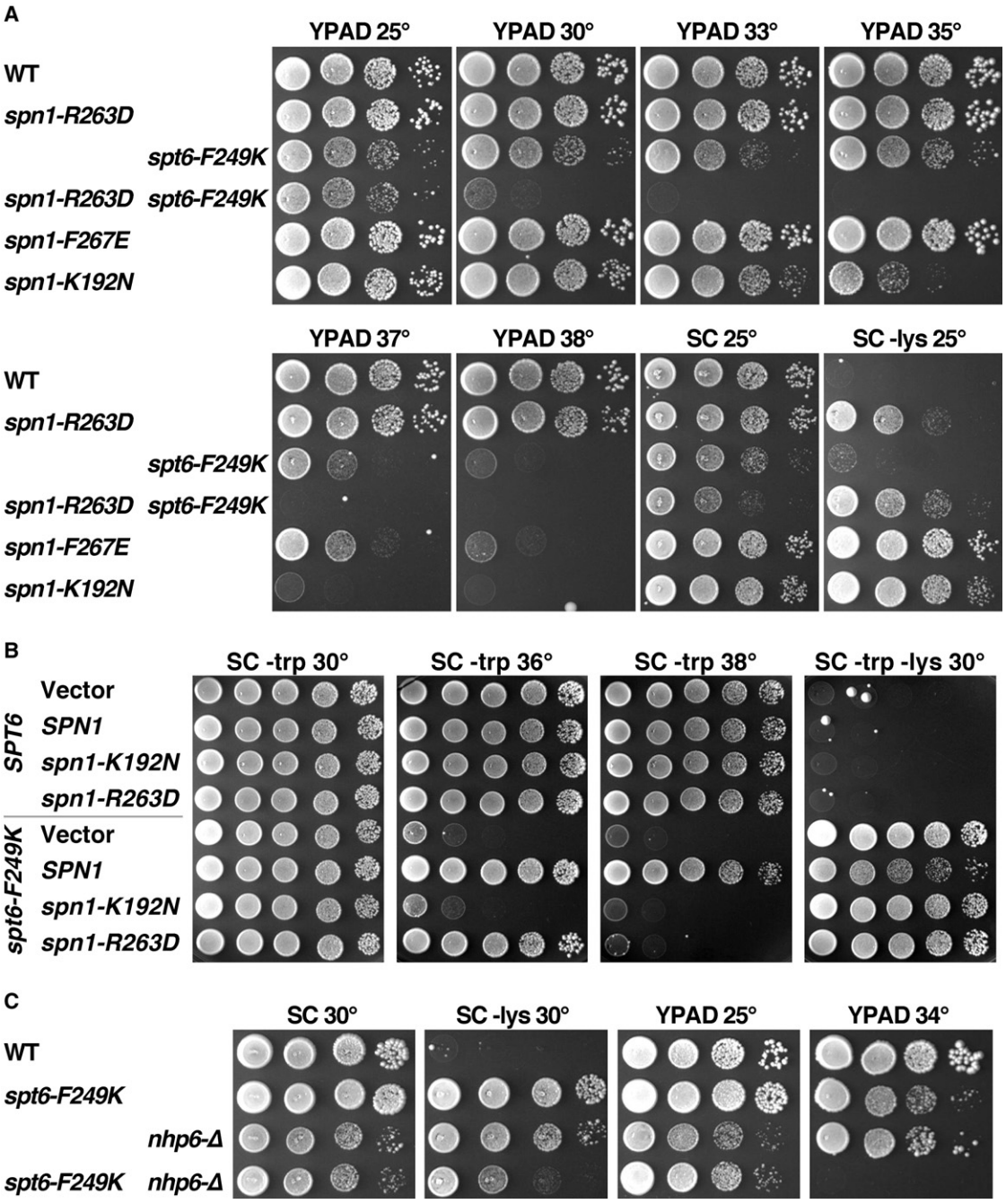

Figure 5. The Spn1-Spt6 Interaction Is Significant for the Essential Activities of Each Protein In Vivo

(A) Isogenic strains from the A364a genetic background and with the relevant genotypes indicated (Supplemental Information) were grown to saturation in rich medium, then aliquots of 10-fold serial dilutions were placed on solid medium and incubated as labeled. SC is synthetic medium (complete or lacking tryptophan or lysine as noted) and YPAD is rich medium. Growth on medium lacking lysine reveals the Spt$^-$ phenotype, reporting here on aberrant transcription initiation from the *lys2-128∂* allele. The strain with the *spt6-F249K* allele grows slowly on SC –lys at 25°, but the Spt$^-$ phenotype is more robust at 30° (B).

(B) WT and *spt6-F249K* strains were transformed with a high-copy number vector or the same vector carrying the version of *SPN1* noted (Supplemental Information). Multiple transformants were tested to insure that the phenotypes detected are typical, then one clone of each was grown to saturation in synthetic medium lacking tryptophan to select for retention of the plasmids. Aliquots of 10-fold serial dilutions were placed on solid synthetic medium as in (A) and incubated as indicated.

(C) As in (A). *nhp6-Δ* indicates deletion of both *NHP6A* and *NHP6B*.

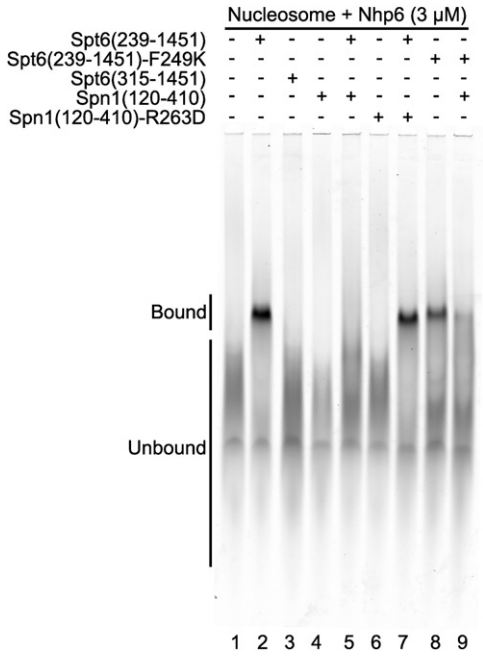

Figure 6. Spt6 Binds Nucleosomes and Is Competed by Spn1

EMSA visualizing the signal from the labeled DNA incorporated into the nucleosomes (Cy5, 633 nm). All reactions included 150 fmoles of nucleosomes, 3 μM Nhp6, and 2 μM of the indicated Spt6 or Spn1 proteins. Migration positions of bound and unbound nucleosomes are indicated. Addition of Spn1 reduced the amount of Spt6-nucleosome complex from 37% of the total signal in lane 2 to 3.2% in lane 5 (9% remaining), but Spn1-R263D only reduced it to 28% (76% remaining). Spt6-F249K formed a lower amount of stable complex (18%), but Spn1 was less effective at inhibiting this (6% bound, or 36% of the original signal remaining comparing lanes 8 and 9) than it was with WT Spt6 (9% of the original signal remaining).

region of Spt6 likely provide a tether whose flexibility may be required to allow the Spn1-Spt6 complex to form in multiple functional contexts.

Spt6 and Spn1 were found to copurify in high-throughput screens (Gavin et al., 2002; Krogan et al., 2002), and further studies suggested that their interaction promotes normal activation of genes regulated after recruitment of RNAPII (Fischbeck et al., 2002; Yoh et al., 2007; Zhang et al., 2008). However, Spt6 and Spn1 have also been implicated in several other distinct and overlapping roles, and each has been implicated in interactions with multiple factors. We have verified a functional interplay between Spt6 and Spn1 proteins in *S. cerevisiae* by demonstrating that cells cannot tolerate certain partial loss-of-function alleles of both genes simultaneously, and by showing that the defects caused by the *spt6-F249K* allele, which impairs binding with Spn1, can be suppressed by overexpressing *SPN1*. Our results therefore show that a short region of Spt6 is important for interacting with Spn1 during at least one of the essential processes mediated by these proteins.

One of the primary functions ascribed to Spt6 is as a histone chaperone that promotes the reassembly of nucleosomes following passage of RNAPII (Adkins and Tyler, 2006; Bortvin and Winston, 1996; Cheung et al., 2008; Kaplan et al., 2003). Spt6 was previously shown to bind histones and to promote nucleosome deposition in vitro (Bortvin and Winston, 1996), and we now show that it can also bind to intact nucleosomes. The dependence of this interaction upon the presence of Nhp6 is consistent with our genetic studies and with an equivalent dependence of the unrelated FACT histone chaperone for its interaction with intact nucleosomes (Formosa et al., 2001). We found that nucleosome binding requires a section of Spt6 that overlaps with the Spn1 binding site, that Spn1 antagonizes Spt6-nucleosome binding in vitro, that either *SPT6* or *SPN1* mutations that affect the Spn1-Spt6 interaction cause the Spt$^-$ phenotype, and that the effects of the *spt6-F249K* allele can be suppressed by overexpressing Spn1. These results show that the Spn1-Spt6 interaction disrupts Spt6-nucleosome binding and that this disruption has a positive role in maintaining normal chromatin. An attractive explanation is that Spn1 is actively engaged in the nucleosome reassembly process, possibly by disengaging Spt6 from nucleosomes to allow multiple rounds of reassembly (see the graphical abstract available online). Another possibility is that Spn1 binding influences the balance between Spt6's functional roles in nucleosome reassembly and mRNA processing. Regardless of the precise mechanistic details, Spn1 appears to be important for Spt6-mediated nucleosome reassembly in vivo.

Nucleosome reassembly is just one of several processes in which Spt6 and Spn1 have been implicated. For example, Spn1, in complex with Spt6, has been reported to interact with a variety of other factors that function in mRNA processing, nucleosome modification, or transcription, including REF1/Aly, Setd2, and RNAPII (Yoh et al., 2007, 2008; Zhang et al., 2008). Our structural data provide insight into how Spn1 might accommodate simultaneous interactions. Spt6 binds against a region of the Spn1 surface that is rich in conserved residues, but other regions of Spn1 display a similar level of conservation and are therefore good candidates for binding surfaces for other proteins (Figure 2C, Figure S1C). This includes residues that are immediately adjacent to the Spt6 binding surface but extend beyond contacts with Spt6, which may indicate that other factors can bind Spn1 cooperatively or competitively with Spt6. Finally, K192, whose mutation to asparagine impairs Spn1 function (Zhang et al., 2008) and appears to function in interactions with RNAPII, is located in a conserved pocket that is formed at the ends of H1, H2, and H4 (Figures 2B and 2C), suggesting another potential binding surface.

In summary, we have determined the structural basis for the interaction between Spn1 and Spt6, and shown that this interaction is important in vivo and that it regulates Spt6-nucleosome binding in vitro. Overall, our data indicate that Spn1 is important for Spt6-mediated nucleosome reassembly, perhaps by regulating the process or by providing a switch that drives disengagement. This does not, however, seem to encompass all of the functional roles in which these two proteins and their interaction with each other participate (Lindstrom et al., 2003; Yoh et al., 2007, 2008; Zhang et al., 2008). Sequence conservation indicates that other surfaces on the Spn1 core domain are good candidates for mediating functionally important interactions. Moreover, interactions with Setd2 and REF1/Aly have been mapped to the N- and C-terminal regions, respectively, which extend beyond the Spn1 core domain and are predicted to be

unstructured (Ward et al., 2004; Yoh et al., 2007, 2008). This use of inherently flexible segments, including the N-terminal region of Spt6 that binds the Spn1 core, may provide a mechanism that allows flexibility in a crowded transcriptional environment.

EXPERIMENTAL PROCEDURES

See the Supplemental Information for protein expression and purification, strains used, strain construction, plasmid construction, and tests of the effects of combining *spn1* and *spt6* mutations.

Crystallization and Structure Determination

All crystals were grown at 20°C by sitting drop vapor diffusion. Se-Spn1 (148–307) drops comprised 2 μl of 8 $mg.mL^{-1}$ protein with 2 μl of well solution (0.1 M Bis-Tris propane [pH 7.0], 1.4 M Li_2SO_4). Native Spn1(148–307) drops comprised two parts 7.5 $mg.mL^{-1}$ protein and one part well solution (0.01 M $MgCl_2$, 0.05 M HEPES [pH 7.0], 1.6 M $[NH_4]_2SO_4$). Spn1(148–293)-Spt6(239–268) drops comprised two parts 13 $mg.mL^{-1}$ protein and one part well solution (0.2 M $Mg[CH_3CO_2]_2$, 0.1 M MES [pH 6.5], 20% PEG 8000). Crystals were cryoprotected in a solution of the reservoir made up with 30% glycerol, and cooled by plunging into liquid nitrogen.

All data were processed using HKL2000 (Otwinowski and Minor, 1997). Phases were determined for Se-Spn1(148–307) by single-wavelength anomalous diffraction. Phenix (phenix.autosol) (Adams et al., 2010) located four out of six possible selenium positions and computed a map into which a model was built. This unrefined model was used in molecular replacement using PHASER (McCoy et al., 2005) to determine the structure of native Spn1(148–307) at 2.15 Å resolution. This subsequently refined model was used to determine the Spn1(148–293):Spt6(239–268) structure by molecular replacement. In all cases, model building, refinement,and validation were performed using Coot (Emsley et al., 2010), Phenix (Adams et al., 2010), and MolProbity (Chen et al., 2010), respectively. Refinement of the Spn1(148–293)-Spt6(239–268) complex included TLS restraints (Painter and Merritt, 2006).

Electrostatic potential surfaces were calculated using APBS (Baker et al., 2001). Figures of molecular structures were generated using PyMol (DeLano, 2002).

Size-Exclusion Chromatography Binding Assay

Purified recombinant proteins were mixed at equimolar concentrations (2 μM) and incubated for 2 hr at 4°C. The protein mixture was concentrated to 15 μM and chromatographed on a 120 ml Superdex 200 16/60 column (GE Healthcare) in 15 mM Tris (pH 7.5), 200 mM NaCl, 5% glycerol, 0.5 mM EDTA, and 2 mM 2-mercaptoethanol.

Isothermal Titration Calorimetry

Amino acid substitutions were made by site-directed mutagenesis and verified by DNA sequencing. Purified recombinant proteins were dialyzed overnight at 4°C against 2 L of degassed ITC buffer (20 mM Tris [pH 7.5], 150 mM NaCl, 5% glycerol, 2 mM 2-mercaptoethanol, 0.5 mM EDTA). Titrations for all reactions were done at 25°C on an iTC200 (Microcal), including an initial injection of 0.4 μl (which was omitted from data analysis), and all injections were spaced 180 s apart. For Spt6(239–1117) reactions, the titrations were carried out with 18 injections of 1.8 μl 76 μM Spn1(148–293) into 8.2 μM Spt6(239–1117). For Spt6(239–268) reactions, the titrations were with 18 injections of 2 μl 74 μM Spt6(239–268) into 8 μM Spn1(148–293). For Spt6-F249K reactions, the titrations were with 18 injections of 1.8 μl 1.52 mM Spt6(239–268)-F249K into 168 μM Spn1(148–293). For Spn1-R263D reactions, the titrations were with 18 injections of 1.8 μl 3.5 mM Spt6(239–268) into 389 μM Spn1(148–293)-R263D. For Spn1-F267E reactions, the titrations were with 18 injections of 2.0 μl 5.2 mM Spt6(239–268) into 578 μM Spn1(148–293)-F267E). In all cases, three independent experiments were performed. Data were analyzed using Origin software (Microcal), and the stoichiometry (*N*), association constant (K_A), and change in enthalpy (ΔH) were obtained by fitting the isotherm to the one-site binding model. Other thermodynamic parameters were calculated using the following relationships:

$$K_A^{-1} = K_D \text{ and } -RT\ln K_A = \Delta H - T\Delta S.$$

Nucleosome Preparation and Gel Mobility Shift Binding Assay

A 146 bp sea urchin 5S rDNA fragment labeled with Cy5 was generated by PCR and gel purified. *Xenopus laevis* histone H2A-S113C was labeled with Oregon Green 488-maleimide and then assembled into nucleosome core particles as described (Xin et al., 2009). Reactions contained 15 nM nucleosomes, 2 μM Spt6 or Spn1 proteins, 100 mM NaCl, 0.8 mg/ml HSA, 9.7% glycerol, and 3 μM S. cerevisiae Nhp6a. Following incubation at 30°C for 15 min, samples were subjected to electrophoresis on native polyacrylamide gels (4.5% acrylamide [acr:bis, 37.5:1], 0.5 X TBE, 5% glycerol, 2 mM $MgCl_2$ at 160 V for 6 hr at 4°C). The gels were scanned using a Typhoon imager at 670 BP30/Red(633 nm) for Cy5-DNA and 520 BP40/Blue(488 nm) for Oregon Green 488-H2A, and the amount of signal in the bound form quantified with ImageQuant Software (GE Health Sciences).

ACCESSION NUMBERS

Coordinates and structure factor amplitudes have been deposited for the Spn1 and Spn1-Spt6 crystal structures have been deposited in the Protein Data Bank under ID codes 3o8z and 3oak, respectively.

SUPPLEMENTAL INFORMATION

Supplemental Information includes one table, four figures, Supplemental Experimental Procedures, and Supplemental References and can be found with this article online at doi:10.1016/j.molcel.2010.11.014.

ACKNOWLEDGMENTS

Portions of this research were carried out at the Stanford Synchrotron Radiation Laboratory, a national user facility operated by Stanford University on behalf of the U.S. Department of Energy, Office of Basic Energy Sciences. The SSRL Structural Molecular Biology Program is supported by the Department of Energy, Office of Biological and Environmental Research, and by the U.S. National Institutes of Health (NIH), National Center for Research Resources, Biomedical Technology Program, and the National Institute of General Medical Sciences. We thank David Stillman and Warren Voth for helpful discussions and Charisse Kettelkamp and Laura McCullough for technical assistance. This work was supported by NIH grants to C.P.H. and T.F.

Received: May 26, 2010
Revised: August 11, 2010
Accepted: September 21, 2010
Published online: November 18, 2010

REFERENCES

Adams, P.D., Afonine, P.V., Bunkoczi, G., Chen, V.B., Davis, I.W., Echols, N., Headd, J.J., Hung, L.W., Kapral, G.J., Grosse-Kunstleve, R.W., et al. (2010). PHENIX: a comprehensive Python-based system for macromolecular structure solution. Acta Crystallogr. D Biol. Crystallogr. *66*, 213–221.

Adkins, M.W., and Tyler, J.K. (2006). Transcriptional activators are dispensable for transcription in the absence of Spt6-mediated chromatin reassembly of promoter regions. Mol. Cell *21*, 405–416.

Andrulis, E.D., Werner, J., Nazarian, A., Erdjument-Bromage, H., Tempst, P., and Lis, J.T. (2002). The RNA processing exosome is linked to elongating RNA polymerase II in Drosophila. Nature *420*, 837–841.

Antczak, A.J., Tsubota, T., Kaufman, P.D., and Berger, J.M. (2006). Structure of the yeast histone H3-ASF1 interaction: implications for chaperone mechanism, species-specific interactions, and epigenetics. BMC Struct. Biol. *6*, 26.

Ardehali, M.B., Yao, J., Adelman, K., Fuda, N.J., Petesch, S.J., Webb, W.W., and Lis, J.T. (2009). Spt6 enhances the elongation rate of RNA polymerase II in vivo. EMBO J. *28*, 1067–1077.

Baker, N.A., Sept, D., Joseph, S., Holst, M.J., and McCammon, J.A. (2001). Electrostatics of nanosystems: application to microtubules and the ribosome. Proc. Natl. Acad. Sci. USA *98*, 10037–10041.

Baniahmad, C., Nawaz, Z., Baniahmad, A., Gleeson, M.A., Tsai, M.J., and O'Malley, B.W. (1995). Enhancement of human estrogen receptor activity by SPT6: a potential coactivator. Mol. Endocrinol. *9*, 34–43.

Becker, R., Loll, B., and Meinhart, A. (2008). Snapshots of the RNA processing factor SCAF8 bound to different phosphorylated forms of the carboxyl-terminal domain of RNA polymerase II. J. Biol. Chem. *283*, 22659–22669.

Bortvin, A., and Winston, F. (1996). Evidence that Spt6p controls chromatin structure by a direct interaction with histones. Science *272*, 1473–1476.

Bucheli, M.E., and Buratowski, S. (2005). Npl3 is an antagonist of mRNA 3′ end formation by RNA polymerase II. EMBO J. *24*, 2150–2160.

Burckin, T., Nagel, R., Mandel-Gutfreund, Y., Shiue, L., Clark, T.A., Chong, J.L., Chang, T.H., Squazzo, S., Hartzog, G., and Ares, M., Jr. (2005). Exploring functional relationships between components of the gene expression machinery. Nat. Struct. Mol. Biol. *12*, 175–182.

Chen, V.B., Arendall, W.B., 3rd, Headd, J.J., Keedy, D.A., Immormino, R.M., Kapral, G.J., Murray, L.W., Richardson, J.S., and Richardson, D.C. (2010). MolProbity: all-atom structure validation for macromolecular crystallography. Acta Crystallogr. D Biol. Crystallogr. *66*, 12–21.

Cheung, V., Chua, G., Batada, N.N., Landry, C.R., Michnick, S.W., Hughes, T.R., and Winston, F. (2008). Chromatin- and transcription-related factors repress transcription from within coding regions throughout the Saccharomyces cerevisiae genome. PLoS Biol. *6*, e277. 10.1371/journal.pbio.0060277.

Clark-Adams, C.D., and Winston, F. (1987). The SPT6 gene is essential for growth and is required for delta-mediated transcription in Saccharomyces cerevisiae. Mol. Cell. Biol. *7*, 679–686.

DeLano, W.L. (2002). The Pymol Molecular Graphics System (Palo Alto, CA: Delano Scientific).

Dengl, S., Mayer, A., Sun, M., and Cramer, P. (2009). Structure and in vivo requirement of the yeast Spt6 SH2 domain. J. Mol. Biol. *389*, 211–225.

Denis, C.L. (1984). Identification of new genes involved in the regulation of yeast alcohol dehydrogenase II. Genetics *108*, 833–844.

Emsley, P., Lohkamp, B., Scott, W.G., and Cowtan, K. (2010). Features and development of Coot. Acta Crystallogr. D Biol. Crystallogr. *66*, 486–501.

Endoh, M., Zhu, W., Hasegawa, J., Watanabe, H., Kim, D.K., Aida, M., Inukai, N., Narita, T., Yamada, T., Furuya, A., et al. (2004). Human Spt6 stimulates transcription elongation by RNA polymerase II in vitro. Mol. Cell. Biol. *24*, 3324–3336.

English, C.M., Adkins, M.W., Carson, J.J., Churchill, M.E., and Tyler, J.K. (2006). Structural basis for the histone chaperone activity of Asf1. Cell *127*, 495–508.

Fischbeck, J.A., Kraemer, S.M., and Stargell, L.A. (2002). SPN1, a conserved gene identified by suppression of a postrecruitment-defective yeast TATA-binding protein mutant. Genetics *162*, 1605–1616.

Formosa, T., Eriksson, P., Wittmeyer, J., Ginn, J., Yu, Y., and Stillman, D.J. (2001). Spt16-Pob3 and the HMG protein Nhp6 combine to form the nucleosome-binding factor SPN. EMBO J. *20*, 3506–3517.

Gavin, A.C., Bosche, M., Krause, R., Grandi, P., Marzioch, M., Bauer, A., Schultz, J., Rick, J.M., Michon, A.M., Cruciat, C.M., et al. (2002). Functional organization of the yeast proteome by systematic analysis of protein complexes. Nature *415*, 141–147.

Gouet, P., Robert, X., and Courcelle, E. (2003). ESPript/ENDscript: extracting and rendering sequence and 3D information from atomic structures of proteins. Nucleic Acids Res. *31*, 3320–3323.

Hartzog, G.A., Wada, T., Handa, H., and Winston, F. (1998). Evidence that Spt4, Spt5, and Spt6 control transcription elongation by RNA polymerase II in Saccharomyces cerevisiae. Genes Dev. *12*, 357–369.

Johnson, S.J., Close, D., Robinson, H., Vallet-Gely, I., Dove, S.L., and Hill, C.P. (2008). Crystal structure and RNA binding of the Tex protein from Pseudomonas aeruginosa. J. Mol. Biol. *377*, 1460–1473.

Kaplan, C.D., Morris, J.R., Wu, C., and Winston, F. (2000). Spt5 and spt6 are associated with active transcription and have characteristics of general elongation factors in D. melanogaster. Genes Dev. *14*, 2623–2634.

Kaplan, C.D., Laprade, L., and Winston, F. (2003). Transcription elongation factors repress transcription initiation from cryptic sites. Science *301*, 1096–1099.

Kaplan, C.D., Holland, M.J., and Winston, F. (2005). Interaction between transcription elongation factors and mRNA 3′-end formation at the Saccharomyces cerevisiae GAL10-GAL7 locus. J. Biol. Chem. *280*, 913–922.

Keegan, B.R., Feldman, J.L., Lee, D.H., Koos, D.S., Ho, R.K., Stainier, D.Y., and Yelon, D. (2002). The elongation factors Pandora/Spt6 and Foggy/Spt5 promote transcription in the zebrafish embryo. Development *129*, 1623–1632.

Kok, F.O., Oster, E., Mentzer, L., Hsieh, J.C., Henry, C.A., and Sirotkin, H.I. (2007). The role of the SPT6 chromatin remodeling factor in zebrafish embryogenesis. Dev. Biol. *307*, 214–226.

Krogan, N.J., Kim, M., Ahn, S.H., Zhong, G., Kobor, M.S., Cagney, G., Emili, A., Shilatifard, A., Buratowski, S., and Greenblatt, J.F. (2002). RNA polymerase II elongation factors of Saccharomyces cerevisiae: a targeted proteomics approach. Mol. Cell. Biol. *22*, 6979–6992.

Li, L., Ye, H., Guo, H., and Yin, Y. (2010). Arabidopsis IWS1 interacts with transcription factor BES1 and is involved in plant steroid hormone brassinosteroid regulated gene expression. Proc. Natl. Acad. Sci. USA *107*, 3918–3923.

Lindstrom, D.L., Squazzo, S.L., Muster, N., Burckin, T.A., Wachter, K.C., Emigh, C.A., McCleery, J.A., Yates, J.R., 3rd, and Hartzog, G.A. (2003). Dual roles for Spt5 in pre-mRNA processing and transcription elongation revealed by identification of Spt5-associated proteins. Mol. Cell. Biol. *23*, 1368–1378.

Ling, Y., Smith, A.J., and Morgan, G.T. (2006). A sequence motif conserved in diverse nuclear proteins identifies a protein interaction domain utilised for nuclear targeting by human TFIIS. Nucleic Acids Res. *34*, 2219–2229.

Liu, Z., Zhou, Z., Chen, G., and Bao, S. (2007). A putative transcriptional elongation factor hIws1 is essential for mammalian cell proliferation. Biochem. Biophys. Res. Commun. *353*, 47–53.

Maclennan, A.J., and Shaw, G. (1993). A yeast SH2 domain. Trends Biochem. Sci. *18*, 464–465.

McCoy, A.J., Grosse-Kunstleve, R.W., Storoni, L.C., and Read, R.J. (2005). Likelihood-enhanced fast translation functions. Acta Crystallogr. D Biol. Crystallogr. *61*, 458–464.

Meinhart, A., and Cramer, P. (2004). Recognition of RNA polymerase II carboxy-terminal domain by 3′-RNA-processing factors. Nature *430*, 223–226.

Natsume, R., Eitoku, M., Akai, Y., Sano, N., Horikoshi, M., and Senda, T. (2007). Structure and function of the histone chaperone CIA/ASF1 complexed with histones H3 and H4. Nature *446*, 338–341.

Neigeborn, L., Celenza, J.L., and Carlson, M. (1987). SSN20 is an essential gene with mutant alleles that suppress defects in SUC2 transcription in Saccharomyces cerevisiae. Mol. Cell. Biol. *7*, 672–678.

Nishiwaki, K., Sano, T., and Miwa, J. (1993). emb-5, a gene required for the correct timing of gut precursor cell division during gastrulation in Caenorhabditis elegans, encodes a protein similar to the yeast nuclear protein SPT6. Mol. Gen. Genet. *239*, 313–322.

Notredame, C., Higgins, D.G., and Heringa, J. (2000). T-Coffee: a novel method for fast and accurate multiple sequence alignment. J. Mol. Biol. *302*, 205–217.

Otwinowski, Z., and Minor, W., eds. (1997). Processing of X-ray Diffraction Data Collected in Oscillation Mode (New York: Academic Press).

Painter, J., and Merritt, E.A. (2006). Optimal description of a protein structure in terms of multiple groups undergoing TLS motion. Acta Crystallogr. D Biol. Crystallogr. *62*, 439–450.

Shen, X., Xi, G., Radhakrishnan, Y., and Clemmons, D.R. (2009). Identification of novel SHPS-1-associated proteins and their roles in regulation of insulin-like

growth factor-dependent responses in vascular smooth muscle cells. Mol. Cell. Proteomics *8*, 1539–1551.

Simchen, G., Winston, F., Styles, C.A., and Fink, G.R. (1984). Ty-mediated gene expression of the LYS2 and HIS4 genes of Saccharomyces cerevisiae is controlled by the same SPT genes. Proc. Natl. Acad. Sci. USA *81*, 2431–2434.

Stillman, D.J. (2010). Nhp6: a small but powerful effector of chromatin structure in Saccharomyces cerevisiae. Biochim. Biophys. Acta *1799*, 175–180.

Vanti, M., Gallastegui, E., Respaldiza, I., Rodriguez-Gil, A., Gomez-Herreros, F., Jimeno-Gonzalez, S., Jordan, A., and Chavez, S. (2009). Yeast genetic analysis reveals the involvement of chromatin reassembly factors in repressing HIV-1 basal transcription. PLoS Genet. *5*, e1000339. 10.1371/journal.pgen.1000339.

Ward, J.J., Sodhi, J.S., McGuffin, L.J., Buxton, B.F., and Jones, D.T. (2004). Prediction and functional analysis of native disorder in proteins from the three kingdoms of life. J. Mol. Biol. *337*, 635–645.

Xin, H., Takahata, S., Blanksma, M., McCullough, L., Stillman, D.J., and Formosa, T. (2009). yFACT induces global accessibility of nucleosomal DNA without H2A-H2B displacement. Mol. Cell *35*, 365–376.

Yoh, S.M., Cho, H., Pickle, L., Evans, R.M., and Jones, K.A. (2007). The Spt6 SH2 domain binds Ser2-P RNAPII to direct Iws1-dependent mRNA splicing and export. Genes Dev. *21*, 160–174.

Yoh, S.M., Lucas, J.S., and Jones, K.A. (2008). The Iws1:Spt6:CTD complex controls cotranscriptional mRNA biosynthesis and HYPB/Setd2-mediated histone H3K36 methylation. Genes Dev. *22*, 3422–3434.

Zhang, L., Fletcher, A.G., Cheung, V., Winston, F., and Stargell, L.A. (2008). Spn1 regulates the recruitment of Spt6 and the Swi/Snf complex during transcriptional activation by RNA polymerase II. Mol. Cell. Biol. *28*, 1393–1403.

Note Added in Proof

An independent study (M.-L. Diebold, M. Koch, E. Loeliger, V. Cura, F. Winston, J. Cavarelli, and C. Romier, EMBO J, 10.1038/emboj.2010.272) has also determined a very similar structure of a Spn1-Spt6 complex; the results of the two studies are highly complementary.

Molecular Cell, Volume *40*

Supplemental Information

Structure and Biological Importance of the Spn1-Spt6 Interaction, and Its Regulatory Role in Nucleosome Binding

Seth M. McDonald, Devin Close, Hua Xin, Tim Formosa, and Christopher P. Hill

Supplemental Information Inventory

Table S1. Thermodynamic parameters of the Spn1-Spt6 interaction.

Related to Figures 1, 4, and S3.

Reaction:	Spt6(239-1117) + Spn1(148-293)	Spt6(239-268) + Spn1(148-293)	[a] Spt6-F249K	[a] Spn1-R263D
N (sites)	[b] 1.01 ± 0.04	1.03 ± 0.01	0.97 ± 0.06	0.98 ± 0.1
K_D (μM)	0.168 ± 0.036	0.169 ± 0.053	10.7 ± 1.5	29.7 ± 6.3
ΔH (kcal mol^{-1})	-8.9 ± 0.6	-9.4 ± 0.7	-8.0 ± 0.5	-2.8 ± 0.2
ΔS (cal mol^{-1} K^{-1})	-0.5 ± 2.5	1.06 ± 2.8	-4.14 ± 2.1	11.3 ± 1.0

[a] Reactions were titrations of Spt6(239-268) into Spn1(148-293) with indicated mutant proteins. Spn1-F267E protein produced no detectable binding at concentrations expected to give a reliable estimate of affinity around 40 μM.

[b] Values reported as mean ± standard deviation and were calculated from three independent experiments of each indicated reaction.

Figure S1. Structural similarity between Spn1 core and proteins that bind RNAPII CTD and conservation of amino acid sequences. Related to Figure 2.

(A) An alignment of Spn1 (gray) and Pcf11 (yellow/green). Structures of the Spn1 core and Pcf11 (Meinhart and Cramer, 2004) and SCAF8 (Becker et al., 2008) were aligned with DALI Lite (Holm and Park, 2000). A population of overlaps of both proteins with Spn1 were obtained that typically displayed Z scores ~6 and RMSD values of 3-4 Å for overlap on ~100 residues. Sequence identity after structural alignment is just 5-10%. Alignments on SCAF8 are essentially identical.

(B) Spn1 surface with the Pcf11-bound RNAPII CTD peptide shown after overlap on the proteins. The Spn1 K192 pocket that has been implicated in interactions with RNAPII (Zhang et al., 2008) is indicated. As indicated in the main text, despite the structural similarity, we did not detect measurable binding of CTD peptides with Spn1.

(C-D) Alignments of homologs of (C) the Spn1 core and (D) the fragment of Spt6 that binds Spn1. S.c. *Saccharomyces cerevisiae*; S.p. *Schizosaccharomyces pombe*; C.e. *Caenorhabditis elegans*; D.m. *Drosophila melanogaster*; D.r. *Danio rerio*; H.s. *Homo sapiens*. Secondary structure is indicated above. Residues that make contact across the interface are indicated with a black square or with an asterisk if they were mutated in this study. Numbering refers to the *S. cerevisiae* proteins. Coloring represents degrees of conservation: dark green and red (high), light green and yellow (medium). Amino acid sequences were aligned using the T-coffee multiple sequence alignment method (Notredame et al., 2000) and slightly adjusted manually in light of the structure. Secondary structure designation was by ESPript (Gouet et al., 2003).

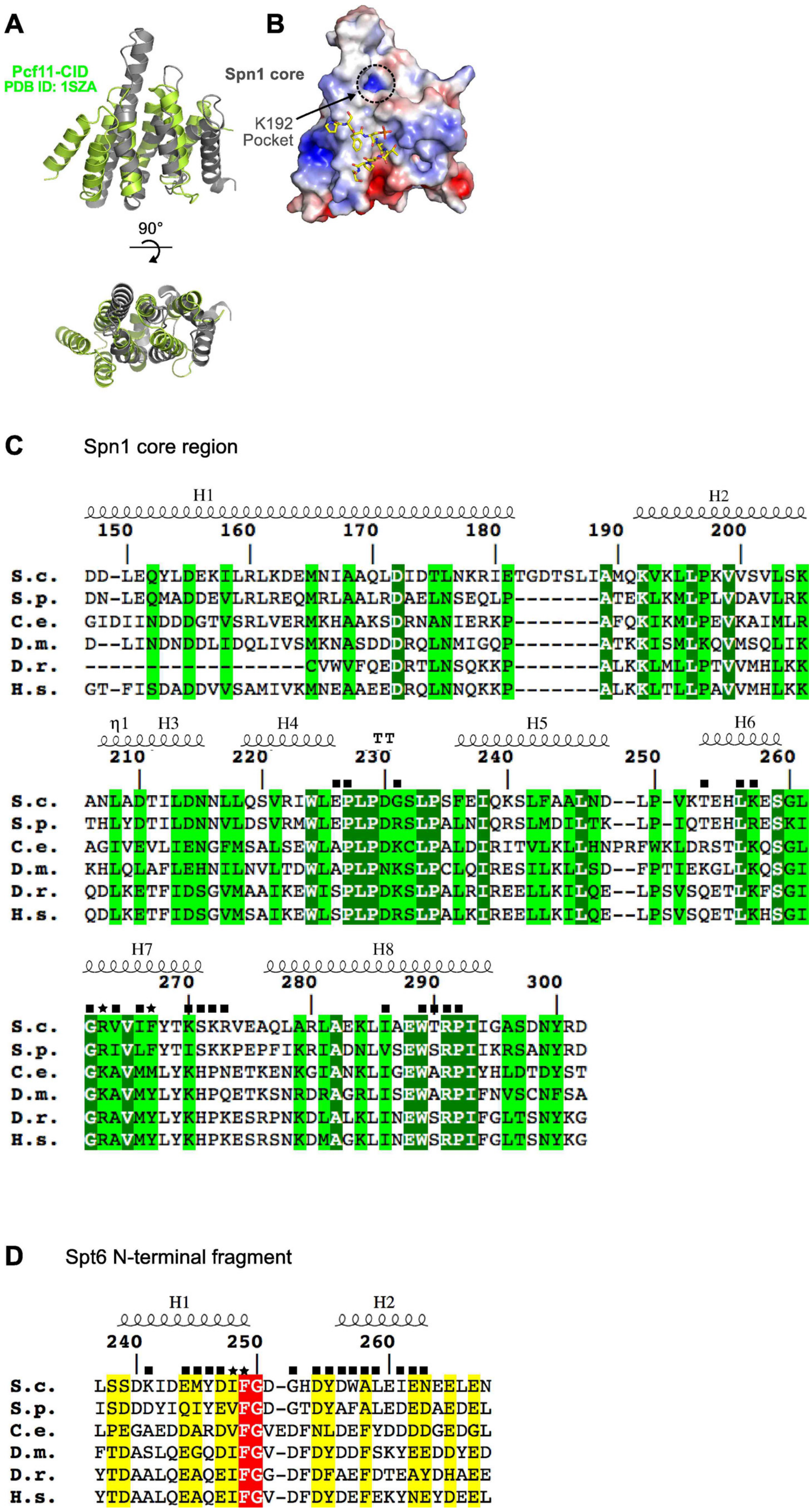

A
Pcf11-CID
PDB ID: 1SZA
90°
B
Spn1 core
K192
Pocket
C
Spn1 core region
H1
H2
150
160
170
180
190
200
S.c. DD-LEQYLDEKILRLKDEMNIAAQLDIDTLNKRIETGDTSLIAMQKVKLLPKVVSVLSK
S.p. DN-LEQMADDEVLRLREQMRLAALRDAELNSEQLP-------ATEKLKMLPLVDAVLRK
C.e. GIDIINDDDGTVSRLVERMKHAAKSDRNANIERKP-------AFQKIKMLPEVKAIMLR
D.m. D--LINDNDDLIDQLIVSMKNASDDDRQLNMIGQP-------ATKKISMLKQVMSQLIK
D.r. ----------------CVWVFQEDRTLNSQKKP-------ALKKLMLLPTVVMHLKK
H.s. GT-FISDADDVVSAMIVKMNEAAEEDRQLNNQKKP-------ALKKLTLLPAVVMHLKK
η1
H3
H4
TT
H5
H6
210
220
230
240
250
260
S.c. ANLADTILDNNLLQSVRIWLEPLPDGSLPSFEIQKSLFAALND--LP-VKTEHLKESGL
S.p. THLYDTILDNNVLDSVRMWLEPLPDRSLPALNIQRSLMDILTK--LP-IQTEHLRESKI
C.e. AGIVEVLIENGFMSALSEWLAPLPDKCLPALDIRITVLKLLHNPRFWKLDRSTLKQSGL
D.m. KHLQLAFLEHNILNVLTDWLAPLPNKSLPCLQIRESILKLLSD--FPTIEKGLLKQSGI
D.r. QDLKETFIDSGVMAAIKEWISPLPDKSLPALRIREELLKILQE--LPSVSQETLKFSGI
H.s. QDLKETFIDSGVMSAIKEWLSPLPDRSLPALKIREELLKILQE--LPSVSQETLKHSGI
H7
H8
270
280
290
300
S.c. GRVVIFYTKSKRVEAQLARLAEKLIAEWTRPIIGASDNYRD
S.p. GRIVLFYTISKKPEPFIKRIADNLVSEWSRPIIKRSANYRD
C.e. GKAVMMLYKHPNETKENKGIANKLIGEWARPIYHLDTDYST
D.m. GKAVMYLYKHPQETKSNRDRAGRLISEWARPIFNVSCNFSA
D.r. GRAVMYLYKHPKESRPNKDLALKLINEWSRPIFGLTSNYKG
H.s. GRAVMYLYKHPKESRSNKDMAGKLINEWSRPIFGLTSNYKG
D
Spt6 N-terminal fragment
H1
H2
240
250
260
S.c. LSSDKIDEMYDIFGD-GHDYDWALEIENEELEN
S.p. ISDDDYIQIYEVFGD-GTDYAFALEDEDAEDEL
C.e. LPEGAEDDARDVFGVEDFNLDEFYDDDDGEDGL
D.m. FTDASLQEGQDIFGV-DFDYDDFSKYEEDDYED
D.r. YTDAALQEAQEIFGG-DFDFAEFDTEAYDHAEE
H.s. YTDAALQEAQEIFGV-DFDYDEFEKYNEYDEEL

Figure S2. Electron density surrounding the Spt6 residues. Related to Figure 3.

Stereoview of the simulated annealing omit-electron density map at 1.5 σ displayed with the final refined model. Density is shown that lies within 4Å of atoms.

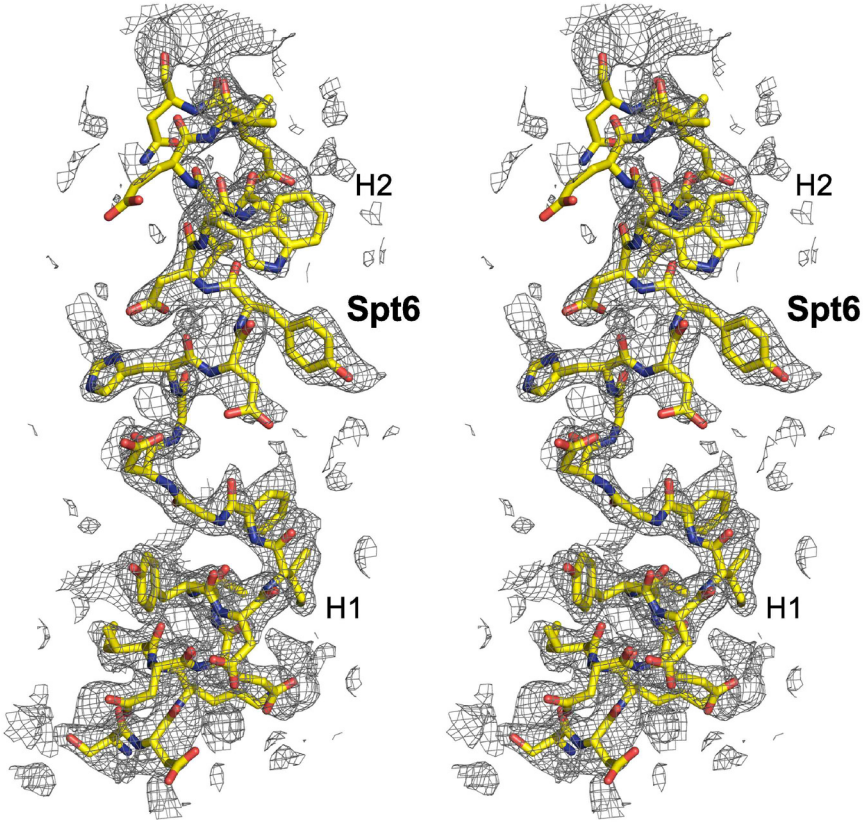

Figure S3. Mutations at the Spn1-Spt6 interface disrupt binding *in vitro*. Related to Figure 4.

Raw ITC data of the indicated titrations for the binding isotherms shown in Figure 4.

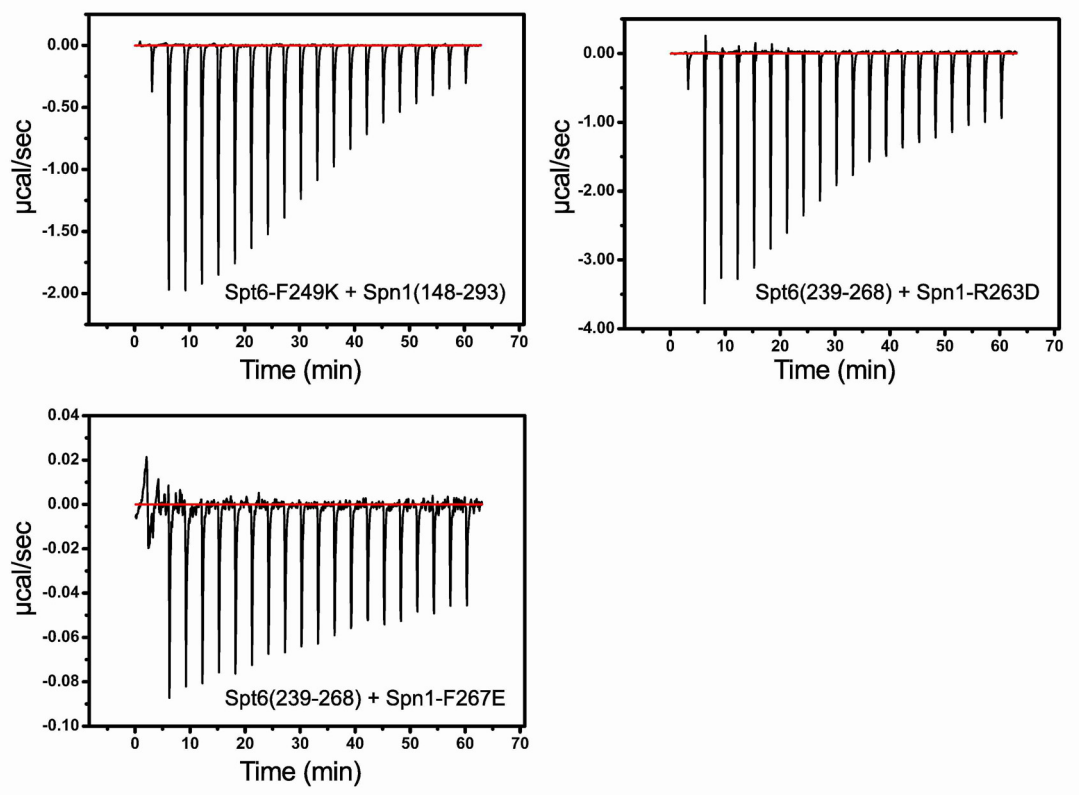

Figure S4. Nhp6 and Spn1 each support functions of Spt6 *in vivo.* Related to Figure 5.

(A) Loss of Nhp6 is detrimental to *spt6* mutants. Strains in the S288C background with the mutations indicated were grown to saturation in rich medium, then 10-fold serial dilutions were spotted to rich medium and incubated for 6 days at 23° C or 3 days at 33° C. Nhp6 is encoded by two very similar genes, *NHP6A* and *NHP6B*, so "*nhp6*-Δ" indicates deletion of both genes. *spt6-1004* is an internal deletion of the helix-hairpin-helix domain within the Tex-like core (Kaplan et al., 2005), *spt6-50* (K1274stop) is a premature termination of the C-terminal domain (deletion of 1274-1451), and spt6-14 is an S952F substitution (F Winston, personal communication); none of these alleles directly affect the Spn1-Spt6 interface. The growth defects caused by these three standard alleles of *SPT6* are all enhanced by loss of Nhp6, especially at elevated temperatures (rows 4, 8, 12), indicating that Nhp6 supports an essential function of Spt6 *in vivo*.

(B, C) As in panel A except the *spn1-F267E* and *spn1-R263D* alleles affecting the Spn1-Spt6 interface are tested in the A364a genetic background. Combining *nhp6*-Δ and *spn1* mutations has more subtle and variable effects, with *spn1-F267E* partially suppressing the growth defect caused by *nhp6*-Δ at 30°, but the double mutant being more impaired than single mutants at 37°. *spn1-R263D* also slightly suppressed *nhp6*-Δ at 30° but did not enhance the Ts- phenotype. These results suggest that Nhp6 does not directly support a function of Spn1, consistent with the model that Spn1 interacts with Spt6 only when Spt6 is not interacting with nucleosomes, and Nhp6 is needed only to support the role of Spt6 when it is interacting with nucleosomes. Panel C also shows the effect of the *spn1-R263A* allele (similar in effect to R263D), and the *spt6-I248K, F249K* double mutation (more severe than F249K alone).

(D) Combining partially defective alleles of *SPN1* and *SPT6* can cause synthetic lethality. Isogenic strains in the A364a genetic background with the *spn1-F267E* or *spn1-K192N* alleles were mated to a strain with the *spt6-F249K* mutation and the diploid was transformed with low copy plasmids with the *URA3* gene and either the *SPT6* or *SPN1* genes (YCp *URA3 SPT6* is shown). Haploid segregants with both *spn1* and *spt6* mutations were obtained after sporulation but were unable to grow on medium containing 5-FOA, indicating that either single mutation is tolerable but the combination of either *spn1* mutation with *spt6-F249K* is lethal. Similar tests also showed that *spn1-K192N* is lethal when combined with either *spt6-1004* or *spt6-F249K* in the S288C background (not shown).

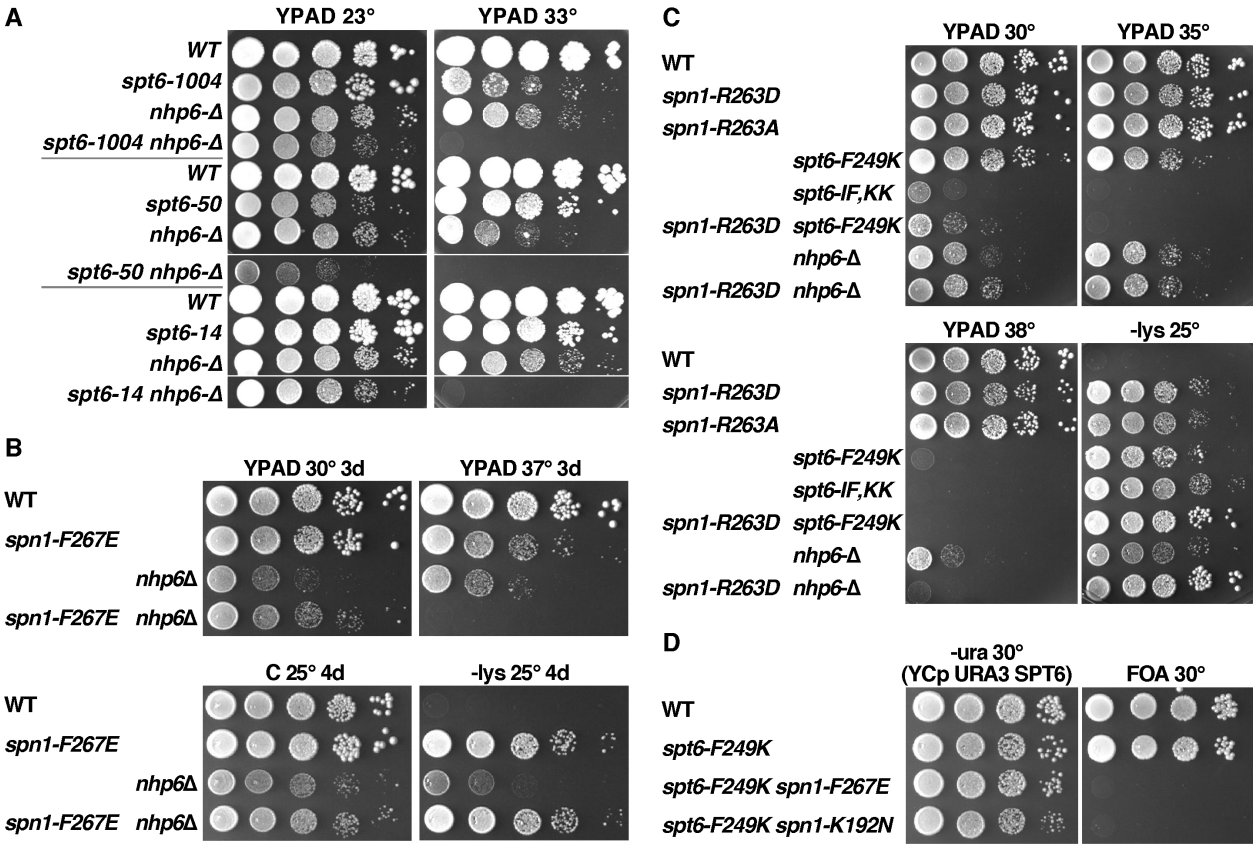

SUPPLEMENTAL EXPERIMENTAL PROCEDURES

Protein Expression and Purification

Coding sequences for full-length *S. cerevisiae* Spn1 and Spt6 proteins were amplified from genomic DNA and inserted into pET151-D-TOPO Amp expression vectors (Invitrogen) containing an N-terminal hexahistidine tag and TEV protease cleavage site. Site-directed mutagenesis was used to insert termination codons to generate C-terminally truncated constructs, while N-terminal truncations were cloned by amplification from the full-length plasmids and subsequent TOPO reaction. Proteins were expressed in *E. coli* BL21-codonplus-(DE3)-RIL cells (Stratagene) in ZY-5052 autoinduction media (Studier, 2005) at 37°C for 5 h and then at 19°C until saturated. For Spn1(148-307) and Spn1(148-293), expression was in LB media at 37°C with induction by 1 mM IPTG at an OD_{600} of 1.0, with subsequent incubation at 19°C for 5 hours. Harvested cell pellets were stored at -80°C.

Cell pellets were thawed, resuspended in lysis buffer (50 mM Tris pH 7.5, 500 mM NaCl, 5% glycerol, and 15 mM imidazole) in the presence of protease inhibitors and lysozyme, and sonicated. Following clarification by centrifugation (29,000xg, 45 min), soluble fractions were applied to Ni-NTA agarose resin (Qiagen) and eluted with 300 mM imidazole (100 mM NaCl). The N-terminal hexahistidine tags of the Spn1 proteins were then removed with TEV protease and any uncleaved protein removed by passage over an Ni-NTA column. Subsequently, Spt6(239-268) was applied to an anion-exchange column (5 mL HiTrap Q HP, GE Healthcare) and eluted with a NaCl gradient. Spn1 proteins were chromatographed on Heparin (5 mL HiTrap Heparin HP, GE Healthcare) and Q columns and collected in the flow through. The Spn1(148-293)-Spt6(239-268) complex was prepared by mixing equimolar amounts, removing

the N-terminal hexahistidine tag of Spt6(239-268) with TEV protease, and passing over a Ni-NTA column. The final purification step for Spn1(148-307) and for the complex was size-exclusion chromatography (Superdex 200 16/60, GE Healthcare) in 15 mM Tris pH 7.5, 100 mM NaCl, 5% glycerol, 0.5 mM EDTA, and 2 mM 2-mercaptoethanol. Selenomethionine-substituted Spn1(148-307) was expressed as described (Studier, 2005) and purified as for the native protein.

Strains Used

A364a background

Fig 5A	
8127-7-4	*MATa ura3-Δ0 leu2-Δ0 trp1-Δ2 his3 lys2-128∂*
8824-1-1	*MATa ura3-Δ0 leu2-Δ0 trp1-Δ2 his3 lys2-128∂ spn1-R263D(TRP1, +49)*
8791-13-3	*MATa ura3-Δ0 leu2-Δ0 trp1-Δ2 his3 lys2-128∂ spt6-F249K(KanMX, -424)*
8834-3-3	*MATa ura3-Δ0 leu2-Δ0 trp1-Δ2 his3 lys2-128∂ spn1-R263D(TRP1, +49) spt6-F249K(KanMX, -424)*
8824-1-2	*MATa ura3-Δ0 leu2-Δ0 trp1-Δ2 his3 lys2-128∂ spn1-F267E(TRP1, +49)*
8768	*MATa ura3-Δ0 leu2-Δ0 trp1-Δ2 his3 lys2-128∂ spn1-K192N*
Fig 5B	
8127-7-4	*MATa ura3-Δ0 leu2-Δ0 trp1-Δ2 his3 lys2-128∂*
8762-5-3	*MATa ura3-Δ0 leu2-Δ0 trp1-Δ2 his3 lys2-128∂ spt6-F249K(URA3, -424)*
Fig 5C	
8127-7-4	*MATa ura3-Δ0 leu2-Δ0 trp1-Δ2 his3 lys2-128∂*
8762-5-3	*MATa ura3-Δ0 leu2-Δ0 trp1-Δ2 his3 lys2-128∂ spt6-F249K(URA3, -424)*
8359-2-4	*MATa ura3 leu2 trp1 his3 lys2-128∂ nhp6a-Δ(::KanMX) nhp6b-Δ(::HIS3)*
8772-3-4	*MATa ura3 leu2 trp1 his3 lys2-128∂ nhp6a-Δ(::KanMX) nhp6b-Δ(::HIS3) spt6-F249K(URA3, -424)*
Fig S4B	
8151-1-1	*MATa ura3-Δ0 leu2-Δ0 trp1-Δ2 his7 lys2-128∂*
8824-4-3	*MATa ura3-Δ0 leu2-Δ0 trp1-Δ2 his7 lys2-128∂ spn1-F267E(TRP1, +49)*
8359-2-4	*MATa ura3 leu2 trp1 his3 lys2-128∂ nhp6a-Δ(::KanMX) nhp6b-Δ(::HIS3)*
8838-1-4	*MATa ura3 leu2 trp1 his3 lys2-128∂ nhp6a-Δ(::KanMX) nhp6b-Δ(::HIS3) spn1-F267E(TRP1, +49)*
Fig S4C	
8151-1-1	*MATa ura3-Δ0 leu2-Δ0 trp1-Δ2 his7 lys2-128∂*
8824-6-1	*MATa ura3-Δ0 leu2-Δ0 trp1-Δ2 his7 lys2-128∂ spn1-R263D(TRP1, +49)*
8824-5-2	*MATa ura3-Δ0 leu2-Δ0 trp1-Δ2 his7 lys2-128∂ spn1-R263A(TRP1, +49)*
8791-9-3	*MATa ura3-Δ0 leu2-Δ0 trp1-Δ2 his7 lys2-128∂ spt6-F249K(KanMX, -424)*
8763-7-3	*MATa ura3-Δ0 leu2-Δ0 trp1-Δ2 his7 lys2-128∂ spt6-I248K, F249K(URA3, -424)*
8834-2-3	*MATa ura3-Δ0 leu2-Δ0 trp1-Δ2 his7 lys2-128∂ spn1-R263D(TRP1, +49) spt6-F249K(KanMX, -424)*
8359-2-4	*MATa ura3 leu2 trp1 his3 lys2-128∂ nhp6a-Δ(::KanMX) nhp6b-Δ(::HIS3)*
8835-7-3	*MATa ura3 leu2 trp1 his3 lys2-128∂ nhp6a-Δ(::KanMX) nhp6b-Δ(::HIS3) spn1-R263D(TRP1, +49)*
Fig S4D	
8839-6-2	*MATα ura3-Δ0 leu2-Δ0 trp1-Δ2 his7 lys2-128∂ pLK04 (YCp URA3 SPT6)*

8839-2-3	*MATa ura3-Δ0 leu2-Δ0 trp1-Δ2 his7 lys2-128∂ spt6-F249K(KanMX, -424) pLK04 (YCp URA3 SPT6)*
8839-6-4	*MATa ura3-Δ0 leu2-Δ0 trp1-Δ2 his3 lys2-128∂ spn1-F267E(TRP1, +49) spt6-F249K(KanMX, -424) pLK04 (YCp URA3 SPT6)*
8791-6-4	*MATa ura3-Δ0 leu2-Δ0 trp1-Δ2 his7 lys2-128∂ spn1-K192N spt6-F249K(KanMX, -424) pLK04 (YCp URA3 SPT6)*

S288C background

Fig S4A	
8165-12-2	*MATa leu2 trp1-Δ63 ura3 his4-912∂ lys2-128∂*
8165-1-1	*MATa leu2 trp1-Δ63 ura3 his4-912∂ lys2 FLAG-spt6-1004*
8165-2-4	*MATa leu2 trp1-Δ63 ura3 his4-912∂ lys2-128∂ nhp6a-Δ(::URA3) nhp6b-Δ(::LEU2)*
8165-8-4	*MATa leu2 trp1-Δ63 ura3 his4-912∂ lys2-128∂ FLAG-spt6-1004 nhp6a-Δ(::URA3) nhp6b-Δ(::LEU2)*
8164-1-1	*MATa leu2 trp1-Δ63 ura3 his4-912∂ lys2-128∂*
8164-3-3	*MATa leu2 trp1-Δ63 ura3 his4-912∂ lys2-128∂ spt6-50*
8164-9-2	*MATa leu2 trp1-Δ63 ura3 his4-912∂ lys2-128∂ nhp6a-Δ(::URA3) nhp6b-Δ(::LEU2)*
8164-10-4	*MATa leu2 trp1-Δ63 ura3 his4-912∂ lys2-128∂ spt6-50 nhp6a-Δ(::URA3) nhp6b-Δ(::LEU2)*
8142-1-2	*MATa leu2 trp1-Δ63 ura3 his4-912∂ lys2-128∂*
8142-8-1	*MATa leu2 ura3 his4-912∂ spt6-14*
8142-7-2	*MATa leu2 ura3 his4-912∂ lys2-128∂ nhp6a-Δ(::URA3) nhp6b-Δ(::LEU2)*
8142-1-4	*MATa leu2 ura3 his4-912∂ lys2 spt6-14 nhp6a-Δ(::URA3) nhp6b-Δ(::LEU2)*

Strain Construction

The *URA3* gene was inserted 424 bp upstream of the *SPT6* ORF, which is 60 bp downstream of *DAM1*. This site was chosen to minimize potential interference with either of these essential genes, and the insertion itself caused no detectable phenotype in any of our tests. Genomic DNA from this strain was then used as the template in a PCR amplification using one wild type primer 343 bp upstream of the insertion and one mutant primer downstream of the insertion containing the F249K mutation followed by 31 nucleotides of WT sequence. This PCR product was used to transform a WT strain. Ura+ transformants were screened for integration of the F249K mutation, indicating recombination between the PCR product and the genomic DNA in the 31 bp interval between the mutation and the end of the product. The transformation was performed in a diploid strain, which was then sporulated to derive haploids. All Ura+ derivatives displayed a severe growth defect initially in the A364a genetic background (but not in the S288C background), but this became more subtle during subsequent vegetative growth. This does not appear to be due to acquisition of a suppressor mutation, as only a mild growth defect was observed segregating 2:2 with the *URA3* marker in subsequent crosses.

Similarly, the *TRP1* gene was integrated 49 bp downstream of the *SPN1* ORF (which is also 161 bp downstream of the convergently transcribed gene *RPS23B*) without any detected phenotype, and genomic DNA from this strain was used as the template to transfer the *TRP1* gene along with the R263D and F267E mutations to a fresh diploid strain. After confirming the integration of the mutation by DNA sequencing, the diploids were sporulated to produce haploid strains with the desired mutation linked to the *TRP1* marker.

The *spn1-K192N* mutation was introduced into an integrating plasmid carrying the *SPN1* and *URA3* genes (described below), and this plasmid was integrated into a haploid yeast strain to

create a duplication of the *SPN1* locus. Recombinants that popped out the plasmid were obtained by selection on medium containing 5-FOA (Boeke et al., 1987), then these were screened for temperature sensitivity. Successful mutation of the *SPN1* gene without other changes was confirmed by DNA sequencing.

Other strains were derived by standard crosses within isogenic backgrounds.

Plasmid Construction

The integrating vector YIplac211 (Gietz and Sugino, 1988) was digested with BamHI and SacI, then a PCR product containing the *SPN1* ORF along with 332 bp of sequence upstream and 50 bp downstream was inserted. The WT sequence was verified by sequencing, and variants with the K192N and R263D mutations were derived using the Quikchange strategy (Stratagene). The mutated plasmids were digested with KpnI to target integration of the K192N mutation to the *SPN1* locus. The inserts from these plasmids were transferred to the high copy vector YEplac112 (Gietz and Sugino, 1988) for the experiment shown in Figure 5B.

pLK04 containing the *SPT6* gene was constructed by inserting DNA fragments flanking the *SPT6* locus into a low copy vector, then using gap repair from a WT strain to fill in the remainder of the gene. This resulted in a plasmid with 495 bp upstream (including the final 11 bp of the adjacent *DAM1* locus to insure inclusion of the entire intergenic region) and 161 bp downstream of the *SPT6* ORF. The sequence was confirmed by DNA sequencing; pLK04 complemented the lethality of an *spt6*-Δ deletion and the temperature sensitivity of all *spt6* alleles tested, but either *spt6* mutant or *SPT6* WT strains with this low copy version of *SPT6* displayed the Spt^- phenotype. Expression of *SPT6* from the plasmid context is therefore aberrant and is sufficient to cause a defect in regulation of transcription.

Testing the effect of combining *spn1* and *spt6* mutations

Isogenic strains in the A364a genetic background with the *spn1-K192N* and *spt6-F249K* alleles were mated and the diploid was transformed with low copy plasmids with the *URA3* gene and either the *SPT6* or *SPN1* genes. Haploid segregants with both mutations were obtained after sporulation in both cases but were unable to grow on medium containing 5-FOA, indicating that either single mutation is tolerable but the combination of *spn1-K192N* and *spt6-F249K* is lethal. Similar tests also showed that *spn1-K192N* is lethal when combined with either *spt6-1004* or *spt6-F249K* in the S288C background.

SUPPLEMENTAL REFERENCES

Becker, R., Loll, B., and Meinhart, A. (2008). Snapshots of the RNA processing factor SCAF8 bound to different phosphorylated forms of the carboxyl-terminal domain of RNA polymerase II. J Biol Chem *283*, 22659-22669.

Boeke, J.D., Trueheart, J., Natsoulis, G., and Fink, G.R. (1987). 5-Fluoroorotic acid as a selective agent in yeast molecular genetics. Methods Enzymol *154*, 164-175.

Gietz, R.D., and Sugino, A. (1988). New yeast-Escherichia coli shuttle vectors constructed with in vitro mutagenized yeast genes lacking six-base pair restriction sites. Gene *74*, 527-534.

Gouet, P., Robert, X., and Courcelle, E. (2003). ESPript/ENDscript: Extracting and rendering sequence and 3D information from atomic structures of proteins. Nucleic Acids Res *31*, 3320-3323.

Holm, L., and Park, J. (2000). DaliLite workbench for protein structure comparison. Bioinformatics *16*, 566-567.

Kaplan, C.D., Holland, M.J., and Winston, F. (2005). Interaction between transcription elongation factors and mRNA 3'-end formation at the Saccharomyces cerevisiae GAL10-GAL7 locus. J Biol Chem *280*, 913-922.

Meinhart, A., and Cramer, P. (2004). Recognition of RNA polymerase II carboxy-terminal domain by 3'-RNA-processing factors. Nature *430*, 223-226.

Notredame, C., Higgins, D.G., and Heringa, J. (2000). T-Coffee: A novel method for fast and accurate multiple sequence alignment. J Mol Biol *302*, 205-217.

Studier, F.W. (2005). Protein production by auto-induction in high density shaking cultures. Protein Expr Purif *41*, 207-234.

Zhang, L., Fletcher, A.G., Cheung, V., Winston, F., and Stargell, L.A. (2008). Spn1 regulates the recruitment of Spt6 and the Swi/Snf complex during transcriptional activation by RNA polymerase II. Mol Cell Biol *28*, 1393-1403.